Theor Chem Acc (2012) 131:1284
DOI 10.1007/s00214-012-1284-x

REGULAR ARTICLE

Implementation in the Pyvib2 program of the localized mode method and application to a helicene

Vincent Liégeois · Benoît Champagne

Received: 3 July 2012 / Accepted: 21 September 2012

Abstract In this paper, after reviewing key elements for simulating and interpreting IR, Raman, VCD, and ROA spectra, as well as after describing the localized mode procedure, we present a graphical user interface to carry out the normal mode localizations and we illustrate its application on the ROA spectra of the [19]helicene molecule. The overall procedure consists of four steps, and therefore, a specific interface has been designed for each of them. The first and most important part of the procedure is the selection of the mode ensemble under which the localization procedure is performed. Then, during our step-by-step guided tour of the localized mode procedure in Pyvib2, we highlight the importance of the ordering of the localized modes and the importance to set correctly the phase factor between the localized modes. Finally, the vibrational coupling matrix ($\tilde{\boldsymbol{\Omega}}$), the intensity coupling matrix ($\tilde{\boldsymbol{I}}$), and the unitary transformation matrix ($\boldsymbol{U}$) can be analyzed from their representation in the different panels. The ROA spectrum of the [19]helicene molecule is dominated by the positive peaks associated with two normal modes. From the localized mode procedure, we have identified the atomic displacements of these modes as a few-node combination of localized modes characterized by atomic displacements that look like the motion of a "claw".

Published as part of the special collection of articles celebrating theoretical and computational chemistry in Belgium.

V. Liégeois (✉) · B. Champagne
Laboratoire de Chimie Théorique, Facultés Universitaires Notre-Dame de la Paix, rue de Bruxelles, 61, 5000 Namur, Belgium
e-mail: vincent.liegeois@fundp.ac.be

Keywords Vibrational spectroscopy · Raman optical activity · Ab initio calculation · Helicene · Localized mode method

1 Introduction

Vibrational signatures are witnesses of the structure, the reactivity, and the properties of molecules, supramolecules, and polymers. Their large number enables to probe the different moieties and functions of the system whereas it complexifies the spectra, making often difficult a straightforward interpretation. This is why simulation and interpretation tools are receiving more and more interest. About a decade ago, our lab initiated a project on simulating vibrational spectra, looking first at Raman and hyper-Raman spectroscopies [1, 2] and then focusing on sum frequency generation (SFG) [3, 4] and vibrational Raman optical activity (ROA) [5–7]. These approaches were initially based on the time-dependent Hartree-Fock (TDHF) method before electron correlation was treated within density functional theory (DFT) or wavefunction methods. In order to be efficient to unravel experimental spectra, these simulation approaches should, however, be combined with efficient visualization and interpretation tools like the Pyvib2 program [8].

The Pyvib2 program [8], first developed by Fedorovsky in Fribourg university (Switzerland), is a tool to plot and analyze vibrational spectra, and in particular infrared absorption (IR), vibrational circular dichroism (VCD), Raman and ROA spectra. This program was initially designed to display the experimental data from the Raman/ROA spectrometer developed by Hug in Fribourg as well as to represent the calculated spectra from the Gaussian [9] or Dalton [10] packages, providing therefore original tools

Published online: 27 October 2012

to unravel the structure/spectra relationships. Some of its key features are (1) the decomposition scheme [11] introduced by Hug that divides the intensity into group coupling matrices (GCMs) or atomic contribution patterns (ACPs) and (2) the interface to analyze the coupling between normal modes of two similar molecules [12, 13]. This program was released as an open-source program and is used by the scientific community worldwide.

For many years, models have been developed to interpret vibrational spectra, leading to rules of thumb that can be used straightforwardly for a preliminary assignment. Among new methods, the localized mode method developed by Jacob and Reiher [14] is mostly devoted to the analysis of the normal modes of polymer chains, where the localized modes are translated (or rototranslated) along the polymer chain. However, one can also use this procedure to obtain the localized modes associated with systems with point group symmetry. This method consists in localizing the vibrational normal modes through a unitary transformation of the normal modes of one specific band. From this, the total band intensity as well as the coupling between the localized modes that gives rise to the band shape can be analyzed. Unfortunately, this method was, up to now, only implemented in a local python program written by Jacob. Our purpose and the topic of this paper was therefore to extend the functionalities of Pyvib2 by implementing a graphical user interface (GUI) in order to carry out the mode localization and the subsequent analysis. The targets encompass its applicability to (1) any kind of molecules and to (2) a broad range of vibrational spectroscopies. The structure of this new tool implemented into Pyvib2 is presented in this paper together with the theoretical aspects underlying the analysis (Sects. 2, 3). Then, in order to illustrate the procedure and the kind of analysis that can be performed, the ROA signatures of the [19]helicene molecule are analyzed. Owing to their remarkable structural, electronic, and optical properties [15–23], helicenes have attracted a renewed interest. For instance, in a previous study [24], we have found that the ROA spectrum of the [6]helicene molecule was dominated by one positive band at around 1,350 cm^{-1}. Therefore, using this implementation of the localized mode approach, we investigate here the origin of this specific signature for a longer chain. Section 4 provides computational details for the calculation of the vibrational normal modes and the ROA intensities of the [19]helicene molecule. At last, Sect. 5 describes the 4 step procedure: (1) selection of a band of normal modes, (2) mode localization, (3) setting of the phase factor, and (4) analysis of the vibrational and intensity coupling matrices together with the analysis of the specific ROA signature of the [19]helicene molecule, exemplifying the procedure and the kind of results that can be obtained from the GUI interface. Section 6 ends this article by drawing conclusions.

2 Vibrational normal modes and IR, Raman, VCD, and ROA intensities

We introduce here basic aspects of vibrational spectroscopies that will be needed further on to describe the localized mode procedure and their analysis. The vibrational normal modes constitute a basis in which the mass-weighted Hessian, $H^m_{i\alpha,j\beta} = \frac{1}{\sqrt{m_i m_j}}\left(\frac{\partial^2 E}{\partial R_{i\alpha}\partial R_{j\beta}}\right)_0$, is diagonal [25]:

$$\boldsymbol{Q}^T\boldsymbol{H}^m\boldsymbol{Q} = \boldsymbol{H}^q \tag{1}$$

The individual elements of $\boldsymbol{H}^q$ are equal to the squares of the angular frequencies, $H^q_{pp} = \omega_p^2 = 4\ \pi^2\ \nu_p^2$, with ν_p being the pth vibrational frequency. The pth column of the unitary matrix $\boldsymbol{Q}$, denoted $\boldsymbol{Q}_p$, is the pth normal mode in terms of mass-weighted Cartesian coordinates. The components of this mode in terms of Cartesian coordinates $\boldsymbol{Q}^c_p$ is then expressed as $Q^c_{i\alpha,p} = (1/\sqrt{m_i})Q_{i\alpha,p}$. In the matrix terms, the indices i and j denote atomic nuclei while α and β are used for Cartesian components (x, y, z).

Within the harmonic approximation, the Raman, ROA [for a naturally polarized incident light (n) in the scattered circularly polarized (SCP) scheme] [26–28], IR, and VCD [29–32] intensities associated with the pth vibrational normal mode respectively read:

$$\begin{aligned}{}^n\mathrm{d}\sigma(\theta)_{\mathrm{SCP},p} &= \frac{1}{90}\frac{1}{c^4}\omega_p^3\omega_0\frac{\hbar}{2\Delta\omega_p}\underbrace{\frac{1}{16\pi^2\epsilon_0^2}}_{I_p^{\mathrm{Raman}}\ [\mathrm{m^4Kg^{-1}}]}[\mathrm{A}\cdot a_p^2 + \mathrm{B}\cdot\beta_p^2]\,\mathrm{d}\Omega\ [\mathrm{m^2/sr}]\end{aligned} \tag{2}$$

$$\begin{aligned}-\Delta^n\mathrm{d}\sigma(\theta)_{\mathrm{SCP},p} &= \frac{1}{90}\frac{1}{c^4}\omega_p^3\omega_0 \\ &\times\frac{\hbar}{2\Delta\omega_p}\underbrace{\frac{1}{c16\pi^2\epsilon_0^2}}_{I_p^{\mathrm{ROA}}\ [\mathrm{m^4Kg^{-1}}]}[\mathrm{C}\cdot aG'_p + \mathrm{D}\cdot\beta^2_{\mathrm{G}p} + \mathrm{E}\cdot\beta^2_{\mathrm{A}p}]\,\mathrm{d}\Omega\ [\mathrm{m^2/sr}]\end{aligned} \tag{3}$$

$$\int_{\mathrm{band}_p}\epsilon(\bar{\nu})\mathrm{d}\bar{\nu} = I_p^{\mathrm{IR}} = \frac{N_A\pi}{3c\epsilon_0\hbar}\Delta\bar{\nu}_p D_{0\to 1_p}\ [\mathrm{m\ mol^{-1}}] \tag{4}$$

$$\int_{\mathrm{band}_p}\Delta\epsilon(\bar{\nu})\mathrm{d}\bar{\nu} = I_p^{\mathrm{VCD}} = \frac{4N_A\pi}{3c^2\epsilon_0\hbar}\Delta\bar{\nu}_p R_{0\to 1_p}\ [\mathrm{m\ mol^{-1}}] \tag{5}$$

where c is the speed of light in vacuum, $\omega_0 = 2\pi\nu_0$ is the angular frequency of the laser beam, ω_p the angular fre-

quency of the scattered light, $\Delta\omega_p$ ($\Delta\bar{\nu}_p$) corresponds to the vibrational transition associated with the normal coordinate Q_p, ϵ_0 is the electric constant (formerly vacuum permittivity), $\hbar$ is the Planck constant divided by 2π, and N_A is the Avogadro number. $D_{0\to 1p}$ and $R_{0\to 1p}$ are the dipole and rotational strength, respectively, while a_p^2, β_p^2, aG'_p, $\beta_{\mathrm{G}p}^2$, $\beta_{\mathrm{A}p}^2$ are the two Raman and the three ROA invariants. A, B, C, D, and E are multiplicative factors that are function of the scattering angle θ. For instance, for the backward-scattering intensity, they amount to 90, 14, 0, 48, and 16, respectively. The Raman I_p^{Raman} and ROA I_p^{ROA} intensities [underbraced quantities in Eqs. (2) and (3)] are expressed in Å^4/amu (SI units: m^4 Kg^{-1}). These units are obtained while using polarizability volumes [33], that is, the polarizability divided by $4\pi\epsilon_0$. In the following, the Raman and ROA intensities will refer to these quantities instead of the scattering cross sections ${}^n\mathrm{d}\sigma(\theta)_{\mathrm{SCP},\ p}$ and $-\Delta^n\mathrm{d}\sigma(\theta)_{\mathrm{SCP},p}$. The main difference is that I_p^{Raman} and I_p^{ROA} intensities do not depend anymore on the vibrational frequency $\Delta\omega_p$.

The Raman (Eq. 2) and ROA (Eq. 3) invariants require the evaluation of the first-order derivatives of three polarizability tensors: $(\partial\alpha/\partial R_{i\alpha})$, $(\partial A/\partial R_{i\alpha})$, and $(\partial G'/\partial R_{i\alpha})$. A review by Buckingham [34] defines all these polarizabilities. The dipole strength and rotational strength entering into the IR (Eq. 4) and VCD (Eq. 5) intensities require the calculation of the atomic polar tensors (APTs, $\boldsymbol{P}_{i\alpha} = \partial\boldsymbol{\mu}/\partial R_{i\alpha}$) and of the atomic axial tensors (AATs, $\boldsymbol{M}_{i\alpha}$), respectively. The Raman and ROA invariants [11] as well as the dipole and rotational strengths [31] have the form:

$$\begin{aligned} a_p^2 &= \frac{1}{9}\sum_{\mu,\nu}\left(\frac{\partial\alpha_{\mu\mu}}{\partial Q_p}\right)_0\left(\frac{\partial\alpha_{\nu\nu}}{\partial Q_p}\right)_0 \\ &= \sum_{i\alpha}\sum_{j\beta}Q^c_{i\alpha,p}Q^c_{j\beta,p}\underbrace{\frac{1}{9}\sum_{\mu,\nu}\left(\frac{\partial\alpha_{\mu\mu}}{\partial R_{i\alpha}}\right)_0\left(\frac{\partial\alpha_{\nu\nu}}{\partial R_{j\beta}}\right)_0}_{V(a^2)_{i\alpha,j\beta}} \end{aligned} \tag{6}$$

$$\begin{aligned} \beta_p^2 &= \frac{1}{2}\sum_{\mu,\nu}\left[3\left(\frac{\partial\alpha_{\mu\nu}}{\partial Q_p}\right)_0\left(\frac{\partial\alpha_{\mu\nu}}{\partial Q_p}\right)_0 - \left(\frac{\partial\alpha_{\mu\mu}}{\partial Q_p}\right)_0\left(\frac{\partial\alpha_{\nu\nu}}{\partial Q_p}\right)_0\right] \\ &= \sum_{i\alpha}\sum_{j\beta}Q^c_{i\alpha,p}Q^c_{j\beta,p} \\ &\underbrace{\frac{1}{2}\sum_{\mu,\nu}\left[3\left(\frac{\partial\alpha_{\mu\nu}}{\partial R_{i\alpha}}\right)_0\left(\frac{\partial\alpha_{\mu\nu}}{\partial R_{j\beta}}\right)_0 - \left(\frac{\partial\alpha_{\mu\mu}}{\partial R_{i\alpha}}\right)_0\left(\frac{\partial\alpha_{\nu\nu}}{\partial R_{j\beta}}\right)_0\right]}_{V(\beta^2)_{i\alpha,j\beta}} \end{aligned} \tag{7}$$

$$\begin{aligned} aG'_p &= \frac{1}{9}\sum_{\mu,\nu}\left(\frac{\partial\alpha_{\mu\mu}}{\partial Q_p}\right)_0\left(\frac{\partial G'_{\nu\nu}}{\partial Q_p}\right)_0 \\ &= \sum_{i\alpha}\sum_{j\beta}Q^c_{i\alpha,p}Q^c_{j\beta,p}\underbrace{\frac{1}{9}\sum_{\mu,\nu}\left(\frac{\partial\alpha_{\mu\mu}}{\partial R_{i\alpha}}\right)_0\left(\frac{\partial G'_{\nu\nu}}{\partial R_{i\beta}}\right)_0}_{V(aG')_{i\alpha,j\beta}} \end{aligned} \tag{8}$$

$$\begin{aligned} \beta_{\mathrm{G}p}^2 &= \frac{1}{2}\sum_{\mu,\nu}\left[3\left(\frac{\partial\alpha_{\mu\nu}}{\partial Q_p}\right)_0\left(\frac{\partial G'_{\mu\nu}}{\partial Q_p}\right)_0 - \left(\frac{\partial\alpha_{\mu\mu}}{\partial Q_p}\right)_0\left(\frac{\partial G'_{\nu\nu}}{\partial Q_p}\right)_0\right] \\ &= \sum_{i\alpha}\sum_{j\beta}Q^c_{i\alpha,p}Q^c_{j\beta,p} \\ &\underbrace{\frac{1}{2}\sum_{\mu,\nu}\left[3\left(\frac{\partial\alpha_{\mu\nu}}{\partial Q_p}\right)_0\left(\frac{\partial G'_{\mu\nu}}{\partial Q_p}\right)_0 - \left(\frac{\partial\alpha_{\mu\mu}}{\partial Q_p}\right)_0\left(\frac{\partial G'_{\nu\nu}}{\partial Q_p}\right)_0\right]}_{V(\beta^2_{\mathrm{G}})_{i\alpha,j\beta}} \end{aligned} \tag{9}$$

$$\begin{aligned} \beta_{\mathrm{A}p}^2 &= \frac{\omega_0}{2}\sum_{\mu,\nu}\sum_{\lambda,\kappa}\left[\left(\frac{\partial\alpha_{\mu\nu}}{\partial Q_p}\right)_0\left(\frac{\epsilon_{\mu\lambda\kappa}\partial A_{\lambda\kappa\nu}}{\partial Q_p}\right)_0\right] \\ &= \sum_{i\alpha}\sum_{j\beta}Q^c_{i\alpha,p}Q^c_{j\beta,p}\underbrace{\frac{\omega_0}{2}\sum_{\mu,\nu}\sum_{\lambda,\kappa}\left[\left(\frac{\partial\alpha_{\mu\nu}}{\partial Q_p}\right)_0\left(\frac{\epsilon_{\mu\lambda\kappa}\partial A_{\lambda\kappa\nu}}{\partial Q_p}\right)_0\right]}_{V(\beta^2_{\mathrm{A}})_{i\alpha,j\beta}} \end{aligned} \tag{10}$$

$$D_{0\to 1_p} = \frac{\hbar}{2\Delta\omega_p}\sum_{i\alpha}\sum_{j\beta}Q^c_{i\alpha,p}Q^c_{j\beta,p}\sum_{\mu}P_{i\alpha,\mu}P_{j\beta,\mu} \tag{11}$$

$$R_{0\to 1_p} = \hbar^2\sum_{i\alpha}\sum_{j\beta}Q^c_{i\alpha,p}Q^c_{j\beta,p}\Im\left[\sum_{\mu}P_{i\alpha,\mu}M_{j\beta,\mu}\right] \tag{12}$$

In the above summations, the indices μ, ν, λ, and κ are components of the electric or magnetic fields (x, y, z). $\epsilon_{\mu\lambda\kappa}$ is the antisymmetric unit tensor of Levi-Civita. The subscript 0 indicates that the properties are evaluated at the equilibrium geometry.

3 Localization of vibrational normal modes

The localized mode procedure [14] consists in performing a unitary transformation on a subset of k normal modes ($\boldsymbol{Q}^{\mathrm{sub}}$) belonging to a specific band in order to obtain localized modes,

$$\tilde{\boldsymbol{Q}}^{\mathrm{sub}} = \boldsymbol{Q}^{\mathrm{sub}}\boldsymbol{U} \tag{13}$$

where the unitary transformation $\boldsymbol{U}$ is chosen in such a way that it yields the "most localized" modes $\tilde{\boldsymbol{Q}}^{\mathrm{sub}}$, that is, it maximizes a criterion that measures how localized a set of modes $\tilde{\boldsymbol{Q}}^{\mathrm{sub}}$ is. Note that throughout this paper, a tilde is used on all quantities that refer to localized modes instead of vibrational normal modes. Two different localization criteria have been proposed and are available in the program: the "atomic-contribution" and the "distance" criteria [14]. The first one refers to the sum of the squares of the atomic contributions to the modes, while the second is based on the distance between the "centers" of the modes, which can be defined by weighting the atomic coordinates. Nevertheless, both criteria lead to similar patterns of the localized modes.

In the basis of the localized modes, the mass-weighed Hessian is not longer diagonal:

$$\tilde{\boldsymbol{Q}}^{T,\mathrm{sub}}\boldsymbol{H}^{m,\mathrm{sub}}\tilde{\boldsymbol{Q}}^{\mathrm{sub}} = \tilde{\boldsymbol{H}}^{\mathrm{sub}} = \boldsymbol{U}^{T}\boldsymbol{H}^{q,\mathrm{sub}}\boldsymbol{U} \tag{14}$$

The diagonal elements of the matrix $\tilde{\boldsymbol{H}}^{\mathrm{sub}}$ are squares of fictitious angular frequencies $\tilde{H}^{\mathrm{sub}}_{ll} = \tilde{\omega}_l^2 = 4\pi^2\tilde{\nu}_l^2$ of the localized modes l while the off-diagonal elements $\tilde{H}^{\mathrm{sub}}_{lm}$ can be interpreted as the couplings between the localized modes l and m. However, the numerical values of the couplings are not easy to analyze as they refer to squares of angular frequencies instead of vibrational frequencies. Therefore, it is useful to introduce a new quantity, the vibrational coupling matrix $\tilde{\boldsymbol{\Omega}}$, defined as [14]:

$$\tilde{\boldsymbol{\Omega}} = \boldsymbol{U}^{T}\boldsymbol{\Omega}\boldsymbol{U} \tag{15}$$

where $\boldsymbol{\Omega}$ is the diagonal matrix with $\Omega_{pp} = \bar{\nu}_p = \omega_p/(2\pi c)$, the wavenumbers of the vibrational normal modes. As seen in [14], the diagonal elements of the coupling matrix $\tilde{\Omega}_{ll}$ can be interpreted as the wavenumbers of the localized modes, while the off-diagonal elements $\tilde{\Omega}_{lm}$ can be understood as coupling constants. It should be noted that the frequencies of the localized modes obtained as the diagonal elements of $\tilde{\boldsymbol{\Omega}}$ are, in general, different from those calculated as the square root of the diagonal elements of $\tilde{\boldsymbol{H}}^{\mathrm{sub}}$, even if the differences between the two are generally quite small. The maximum difference amounts to 1.2 cm^{-1} in our test case (see below).

We can now write the expression of the Raman, ROA, IR, and VCD intensities associated with these localized modes simply by replacing in Eqs. (6) to (12) the normal mode coordinates by the localized mode coordinates. Similarly, the intensity coupling matrix ($\tilde{\boldsymbol{I}}$) is defined as the intensity between any l and k pair of localized modes:

$$\tilde{I}^{\mathrm{Raman}}_{lm} = \frac{1}{16\pi^2\epsilon_0^2}\sum_{i\alpha}\sum_{j\beta}\tilde{Q}^{c}_{i\alpha,l}\tilde{Q}^{c}_{j\beta,m}[\mathrm{A}\cdot V(a^2)_{i\alpha,j\beta} + \mathrm{B}\cdot V(\beta^2)_{i\alpha,j\beta}][\mathrm{m^4Kg^{-1}}] \tag{16}$$

$$\tilde{I}^{\mathrm{ROA}}_{lm} = \frac{1}{c16\pi^2\epsilon_0^2}\sum_{i\alpha}\sum_{j\beta}\tilde{Q}^{c}_{i\alpha,l}\tilde{Q}^{c}_{j\beta,m}[\mathrm{C}\cdot V(aG')_{i\alpha,j\beta} + \mathrm{D}\cdot V(\beta^2_{\mathrm{G}})_{i\alpha,j\beta} + \mathrm{E}\cdot V(\beta^2_{\mathrm{A}})_{i\alpha,j\beta}]\ [\mathrm{m^4Kg^{-1}}] \tag{17}$$

$$\tilde{I}^{\mathrm{IR}}_{lm} = \frac{N_A}{12c^2\epsilon_0}\sum_{i\alpha}\sum_{j\beta}\tilde{Q}^{c}_{i\alpha,l}\tilde{Q}^{c}_{j\beta,m}\sum_{\mu}P_{i\alpha,\mu}P_{j\beta,\mu}\ [\mathrm{m\ mol^{-1}}] \tag{18}$$

$$\tilde{I}^{\mathrm{VCD}}_{lm} = \frac{4N_A\pi\hbar}{3c^2\epsilon_0}\sqrt{\Delta\bar{\nu}_l\Delta\bar{\nu}_m} \times\sum_{i\alpha}\sum_{j\beta}\tilde{Q}^{c}_{i\alpha,l}\tilde{Q}^{c}_{j\beta,m}\Im\left[\sum_{\mu}P_{i\alpha,\mu}M_{j\beta,\mu}\right]\ [\mathrm{m\ mol^{-1}}] \tag{19}$$

The diagonal elements of this matrix, $\tilde{I}_{ll}$, are referred to as the intensities of the lth localized modes, while the off-diagonal values, $\tilde{I}_{lm}$, are the intensity coupling terms. The intensity coupling matrix $\tilde{\boldsymbol{I}}$ can be used to understand the shapes of the band (i.e., how the intensity of a band is spread over all the normal modes, see also below). Indeed, the intensity associated with each vibrational normal mode (I_p) of one band is related to the intensity coupling matrix $\tilde{\boldsymbol{I}}$ and to the unitary transformation $\boldsymbol{U}$:

$$I_p = \sum_{lm}U_{pl}U_{pm}\tilde{I}_{lm} \tag{20}$$

Since the trace of a matrix is conserved along a unitary transformation (Eq. 20), the total intensity of the band $\sum_p I_p$ is equal to the sum of the intensities of the localized modes, $\sum_l \tilde{I}_{ll}$. Moreover, since the atomic displacements of the localized modes are usually similar, so are their intensities. The total intensity of the band can therefore be investigated simply by analyzing the intensity of one localized mode. For the band shape, the intensity coupling matrix $\tilde{\boldsymbol{I}}$ together with the transformation matrix $\boldsymbol{U}$ (eigenvectors of $\tilde{\boldsymbol{\Omega}}$) describes how the intensities of the localized modes are distributed in the vibrational normal modes. One should note, however, that the intensity coupling matrix $\tilde{I}^{\mathrm{VCD}}_{lm}$ for the VCD intensity depends on the geometric mean of the wavenumbers of the two localized modes l and m. Therefore, Eq. (20) is not strictly fulfilled (neither is the equality between the sum of the intensities over the normal modes and the localized modes) even if the deviation is quite small.

4 Computational aspects

In the following, we illustrate the implementation of the localized mode procedure for the analysis of the Raman and ROA spectra of the [19]helicene molecule. The structure as well as the vibrational frequencies and normal modes was determined using the analytical coupled-perturbed Kohn-Sham [35] procedure together with the 6-31G* basis set [36]. The hybrid B3LYP exchange-correlation functional was selected owing to its recognized performance for calculating vibrational frequencies [37]. However, to account for the systematic error due to approximate exchange-correlation functional and anharmonicity effects, a multiplicative factor of 0.96 [37–39] was employed to scale the B3LYP vibrational frequencies.

The geometry derivatives of the three polarizability tensors entering into the Raman and ROA invariants were calculated using the rDPS:3-21G (reduced diffuse polarization function and shell augmented) basis set introduced by Zuber and Hug [40]. It consists of the 3–21++G [41] basis set augmented by a set of p diffuse functions (of exponent 0.2) on the hydrogen atoms. The derivatives are evaluated at the TDHF level for the Cartesian displacements [5] and are transformed afterward into the geometrical derivatives with respect to the vibrational normal coordinates, with the normal coordinates calculated using the CPKS procedure. The calculations were performed using the GAUSSIAN 09 [9] quantum chemistry packages.

While the electron correlation effects in the simulation of vibrational spectroscopies are, till now, most of the time treated by DFT [42–46], other approaches such as coupled-cluster are becoming available [47–49]. Nevertheless, such methods are still in their early stages and are restricted to small molecules. The Pyvib2 program is, however, not limited to any kind of method and can thus analyze the vibrational signatures coming for any quantum chemistry package providing the implementation of a parser.

A typical incident light wavelength of 532 nm was adopted in all optical tensor calculations. The Maxwell–Boltzmann $(1/[1-\mathrm{e}^{(-\hbar\Delta\omega_p/(k_\mathrm{b}T))}])$ factor with $T = 298.15$ K is used to account for the T-dependence of the populations of the vibrational levels.

5 Localized mode method using pyvib2

The procedure to obtain and analyze the localized modes consists of four different steps:

1. The selection of the normal modes that constitute an ensemble (a band) on which we perform the unitary transformation.
2. The mode localization for a given choice of localized criterion (the atomic-contribution or the distance criterion).
3. The setting of the phase factor for each localized mode.
4. The analysis of the vibrational and intensity coupling matrices.

Each of these steps requires a specific input from the user and therefore a specific graphical interface has been developed for each step.

5.1 Determination of the normal mode ensemble

As explained earlier, the localization procedure consists in performing a unitary transformation on a subset of normal

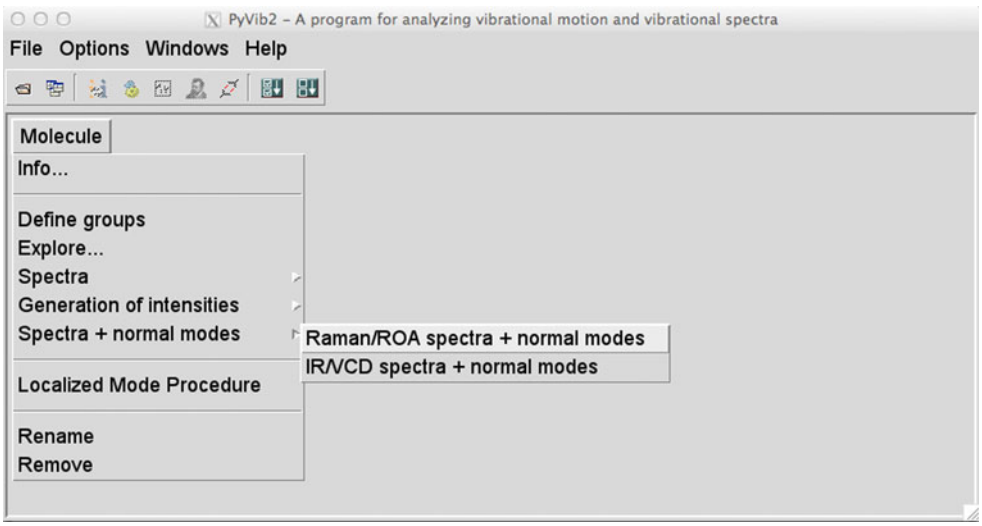

Fig. 1 Screenshot of the options available for analyzing a molecule

modes that belong to a band. This means that we need to select an ensemble of normal modes having similar atomic displacements along the chain, though different phases between the different units of the chain. Most of the time, these modes have similar wavenumbers, but for molecules constituted of only carbon and hydrogen atoms, the frontier between two successive bands can be difficult to assess. Nevertheless, the interface enables to visualize simultaneously the vibrational normal modes and the simulated Raman and ROA spectra. One should note that a similar interface has also been developed for the IR and VCD spectra.

After loading the file into the program, different options are available, see Fig. 1. The `Explore` option loads a window to represent the atomic displacements of the vibrational normal modes, while the `Spectra` option displays the various vibrational spectra. The `Generation of Intensities` option uses the decomposition scheme [11] and renders the group coupling matrices (GCMs) and the atomic contribution patterns (ACPs). The

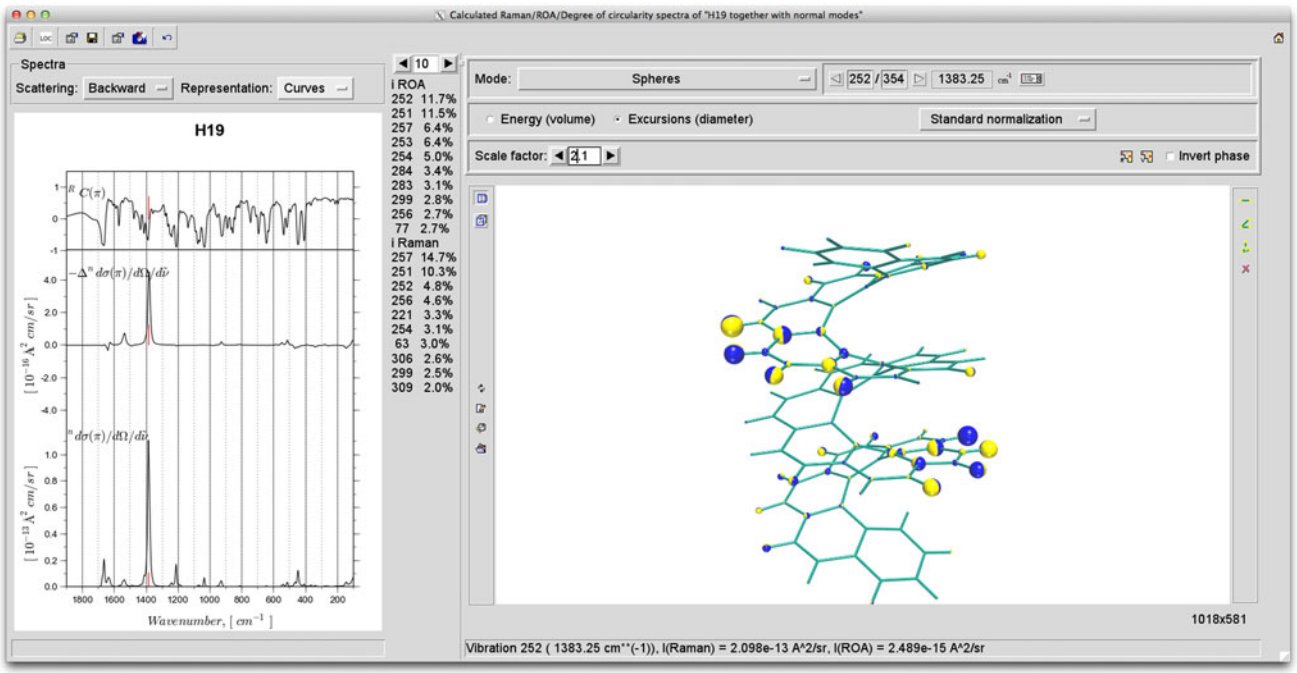

Fig. 2 Screenshot of the window that plots the spectra together with the representation of the atomic displacements of a selected vibrational normal mode

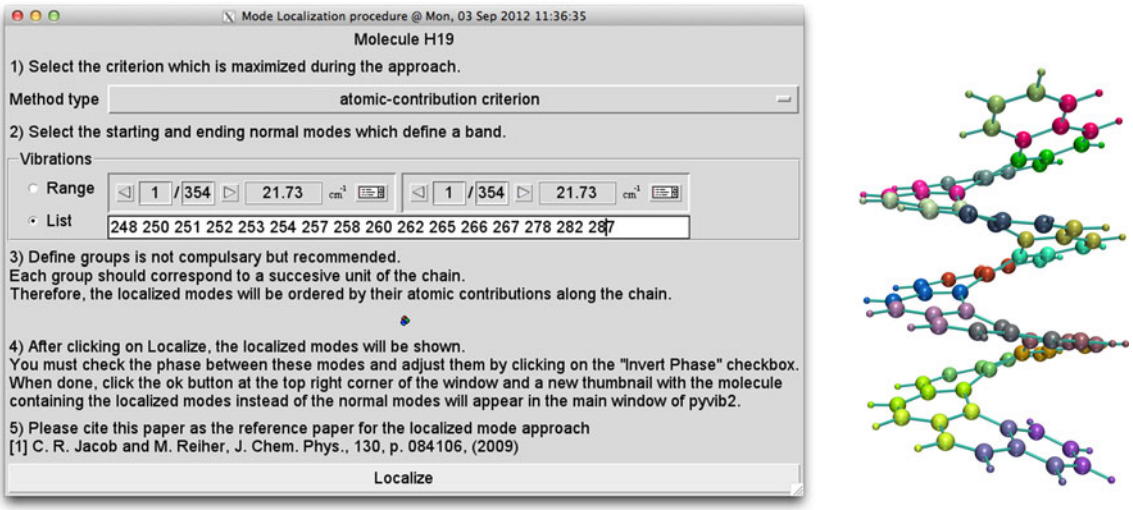

Fig. 3 *Left* Screenshot of the window to launch the "localized mode procedure"; *Right* groups definition

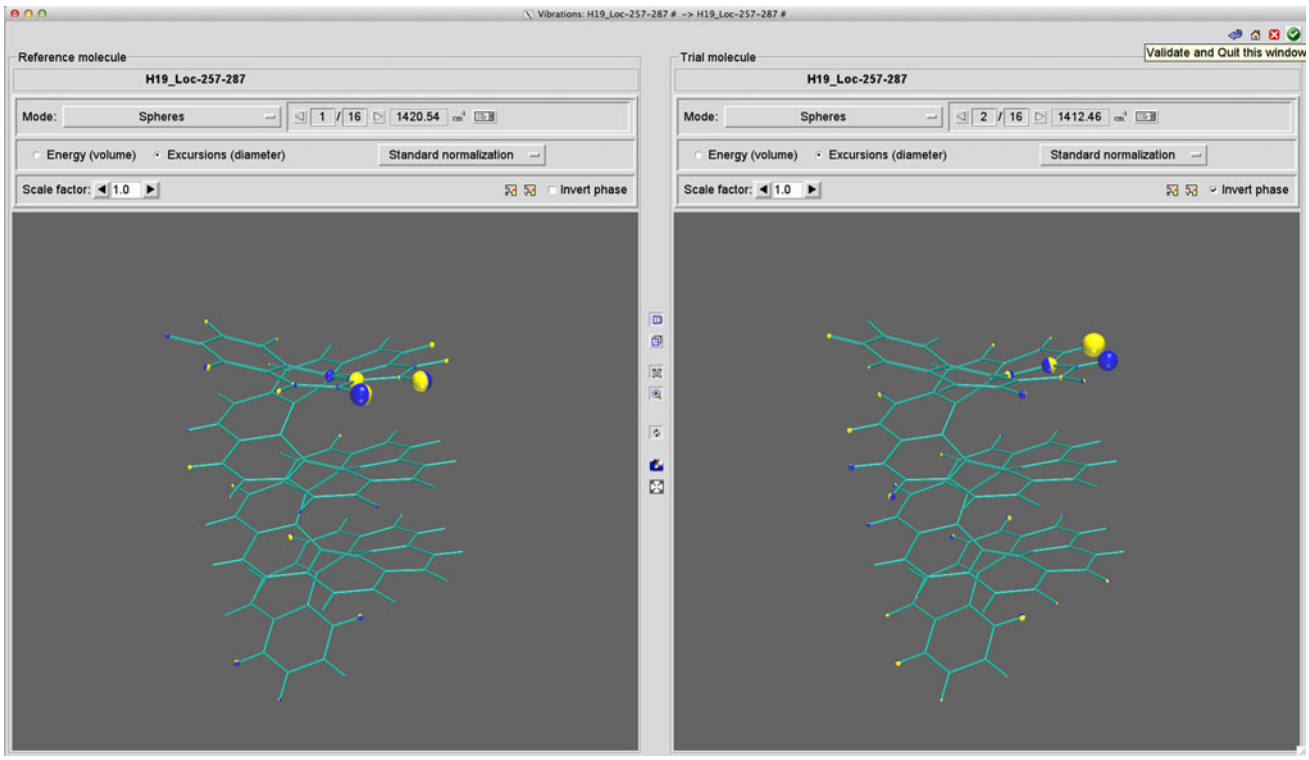

Fig. 4 Screenshot of the window to set the phase factors on the localized modes

`Spectra normal modes` option displays a window to analyze simultaneously the spectra with the normal modes. Figure 2 is an example of such window where mode 252 is selected. On the left, one can see the ROA (middle) and Raman (bottom) spectra together with the degree of circularity (top). In both spectra, the red bars indicate the intensity of the selected sketched mode. The list displayed in the center of the window gives the most intense modes for both the Raman and ROA together with the percentage of their intensity relative to the sum of the intensity of the modes that appears within the wavenumber range of the spectra. For the [19]helicene molecule, the Raman and ROA spectra are dominated by two positive peaks corresponding to modes 251 and 252, which belong to one intense positive band. This signature is similar to the one observed previously for a smaller [6]helicene [24]. On the right side of the window, the atomic displacements of the selected mode are displayed using spheres on each atom. The direction of the displacement of an atom is given by the line joining the two poles of different color while the magnitude of the displacement is given by the radius of the sphere. The atomic displacements associated with the most intense mode (mode 252) involve the stretching of the C–C bond between two neighboring rings and the wagging of two hydrogen atoms at the exterior of the helicene close to the C–C stretching bond. The displacements of these two H atoms and these C atoms look therefore like a claw. The same displacement is found in every junction of two neighboring rings, some of them with the same phase and some with the opposite phase. This same pattern is also found in other modes but with different phases between the different sites. As we have 19 rings, we should find something like 18 similar modes. After close inspection of the vibrational normal modes in the vicinity of modes 251 and 252, it was possible to select 16 similar modes. The two missing modes come from the fact that at the extremity of the chain, this "claw" displacements are mixed with the wagging of the H atoms. The 16 modes numbers (and wavenumbers) are 248 (1,378.8 cm^{-1}), 250 (1,379.6 cm^{-1}), 251 (1,381.6 cm^{-1}), 252 (1,383.3 cm^{-1}), 253 (1,384.7 cm^{-1}), 254 (1,387.2 cm^{-1}), 257 (1,389.4 cm^{-1}), 258 (1,392.8 cm^{-1}), 260 (1,397.1 cm^{-1}), 262 (1,403.0 cm^{-1}), 265 (1,415.1 cm^{-1}), 266 (1,426.4 cm^{-1}), 267 (1,438.7 cm^{-1}), 278 (1,502.6 cm^{-1}), 282 (1,526.9 cm^{-1}), 287 (1,556.8 cm^{-1}).

5.2 Localized mode procedure

Figure 3 illustrates the window that launches the localized mode procedure and is obtained after selecting `Localized Mode Procedure` in Fig. 1. The first step in the procedure consists in selecting the localization criterion.

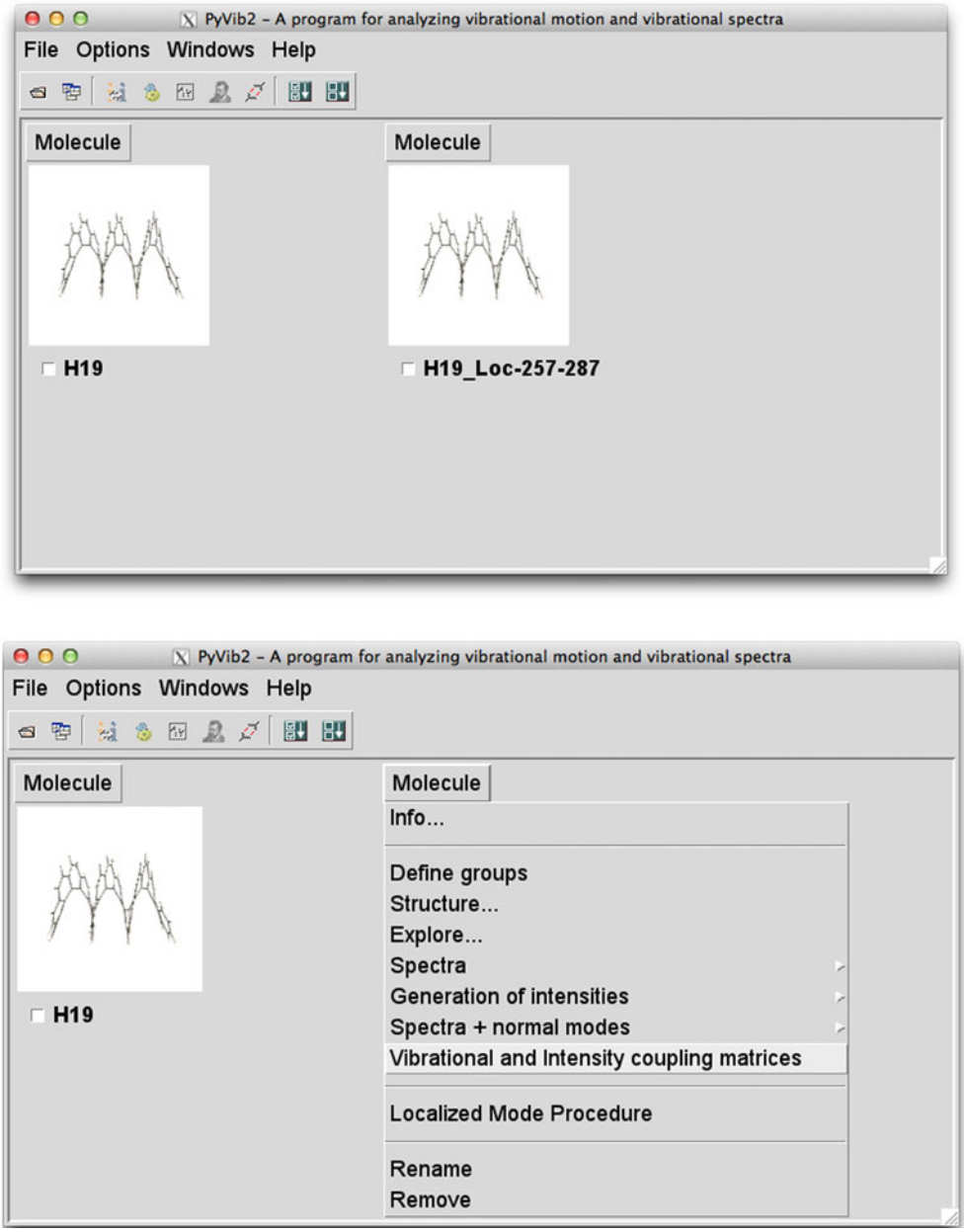

Fig. 5 Screenshot of the main window after the mode localization has been performed

Two choices are available: the "atomic-contribution" criterion and the "distance" criterion [14] but in practice, both of them give similar localized modes and the "atomic-contribution" criterion is used in our example. The next step is to input the ensemble of normal modes among which the localization is performed. Either a continuous range of modes or a list of "individual" modes can be given. In our example, we give the list of the 16 modes reported before. The last step before clicking on the `Localize` button is the definition of groups. This step is not compulsory but highly recommended to help analyzing the vibrational and intensity coupling matrices ($\tilde{\mathbf{\Omega}}$ and $\tilde{\boldsymbol{I}}$). Indeed, by default, the localized modes obtained have no particular order, that is, the first localized mode in the list can have atomic displacements in the middle of the chain, while the next localized mode in the list can have atomic contribution on one extremity of the chain. However, since it is more handy that the successive localized modes involve atomic displacements localized on successive neighboring sites, we therefore define successive groups composed of atoms ranging from one side of the chain to the other. Figure 3 exemplifies the groups defined for the [19]helicene with "group 1" being the 3 C atoms and their H atoms on one extremity of the chain, "group 2" containing 4 C atoms and 2 H atoms just below "group 1", and so one up to "group 20", which contains the last 3 C atoms and their H atoms at the other extremity of the molecule. The localized mode are ordered in such a way that

localized mode 1 has most of its atomic contributions on the first groups while the last localized mode presents atomic contributions mostly centered on the last groups. The number of groups can be different from the number of modes to localize but best orderings are obtained if the atoms constituting a group are the same as those which contribute to the localized modes. This is the reason why the different groups (except the two terminal groups) are made of 4 C atoms and two H atoms, similar to the "claw" displacement corresponding to the normal mode pattern. It is important to notice that the group definition does not influence the generation of the localized mode (only the criterion does) but only provides a way to order them with respect to their position along the chain.

5.3 Set the phase factors on the localized modes

In addition to the ordering of the localized mode, it is important to set the correct phase factor on the localized modes. Indeed, in the analysis, the localized modes constitute a basis set in which each normal mode can be expressed. For instance, the sign of the vibrational coupling between two localized modes is changed if their relative phase is inverted. It is therefore crucial that two localized modes contain similar atomic displacements (without phase shift) but translated (or rototranslated) to the next unit of the chain. However, since the normal mode (as eigenvectors of the mass-weighted Hessian) are not affected by a change of sign of all their contributions, so are the localized modes. Therefore, at the end of the localized mode procedure, a first attempt to set the phase is made by defining the vibrational coupling between two successive neighbors to be positive. Nevertheless, one cannot predict the sign of these couplings, and we therefore need to confirm manually the phase factor for all the localized modes relative to one localized mode taken as reference. Figure 4 shows the interface that was developed for this purpose. The left panel represents the atomic displacements of mode 1 taken as reference (any other mode could have been chosen), while the right panel shows the atomic displacements of another mode. In this particular example, in order to obtain in-phase atomic displacements for modes 1 and 2, the `Invert phase` box was checked. For all the modes except the reference one, the atomic displacements have to be examined and the `Invert phase` box checked if required. When all the modes are inspected, we can click on the top right button that says `Validate and Quit this window`. A new "thumbnail" with the molecule will be created on the main window (Fig. 5). This molecule is different from the original one by the fact that the transformation matrix between the Cartesian coordinates and the mode coordinates is the $\tilde{\boldsymbol{Q}}_l$ matrix, which defines the set of localized modes. The same analyses as for the original molecule can be conducted here, but wherever normal modes are involved ($\boldsymbol{Q}_p$), the localized modes ($\tilde{\boldsymbol{Q}}_l$) are used instead. For instance, using the `Spectra` option will plot the peaks associated with the localized modes (Eqs. 16–19). Moreover, an additional option is available under the name `Vibrational and Intensity coupling matrices` which provides a new window (Figs. 6, 7, 8, 9) with four panels to analyze the localized modes.

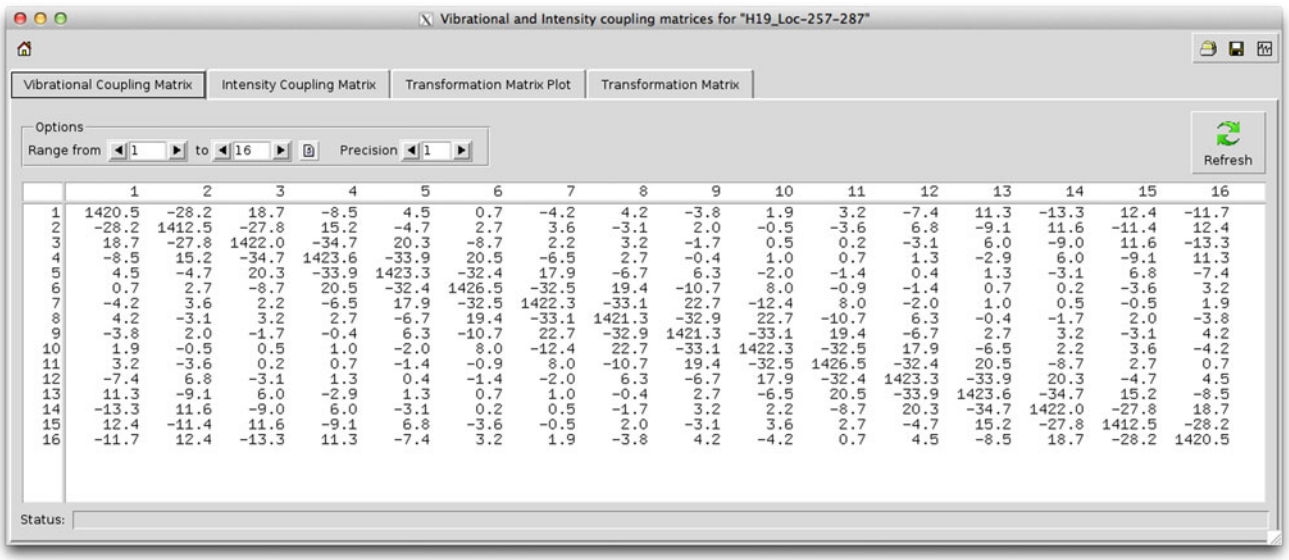

	1	2	3	4	5	6	7	8	9	10	11	12	13	14	15	16
1	1420.5	-28.2	18.7	-8.5	4.5	0.7	-4.2	4.2	-3.8	1.9	3.2	-7.4	11.3	-13.3	12.4	-11.7
2	-28.2	1412.5	-27.8	15.2	-4.7	2.7	3.6	-3.1	2.0	-0.5	-3.6	6.8	-9.1	11.6	-11.4	12.4
3	18.7	-27.8	1422.0	-34.7	20.3	-8.7	2.2	3.2	-1.7	0.5	0.2	-3.1	6.0	-9.0	11.6	-13.3
4	-8.5	15.2	-34.7	1423.6	-33.9	20.5	-6.5	2.7	-0.4	1.0	0.7	1.3	-2.9	6.0	-9.1	11.3
5	4.5	-4.7	20.3	-33.9	1423.3	-32.4	17.9	-6.7	6.3	-2.0	-1.4	0.4	1.3	-3.1	6.8	-7.4
6	0.7	2.7	-8.7	20.5	-32.4	1426.5	-32.5	19.4	-10.7	8.0	-0.9	-1.4	0.7	0.2	-3.6	3.2
7	-4.2	3.6	2.2	-6.5	17.9	-32.5	1422.3	-33.1	22.7	-12.4	8.0	-2.0	1.0	0.5	-0.5	1.9
8	4.2	-3.1	3.2	2.7	-6.7	19.4	-33.1	1421.3	-32.9	22.7	-10.7	6.3	-0.4	-1.7	2.0	-3.8
9	-3.8	2.0	-1.7	-0.4	6.3	-10.7	22.7	-32.9	1421.3	-33.1	19.4	-6.7	2.7	3.2	-3.1	4.2
10	1.9	-0.5	0.5	1.0	-2.0	8.0	-12.4	22.7	-33.1	1422.3	-32.5	17.9	-6.5	2.2	3.6	-4.2
11	3.2	-3.6	0.2	0.7	-1.4	-0.9	8.0	-10.7	19.4	-32.5	1426.5	-32.4	20.5	-8.7	2.7	0.7
12	-7.4	6.8	-3.1	1.3	0.4	-1.4	-2.0	6.3	-6.7	17.9	-32.4	1423.3	-33.9	20.3	-4.7	4.5
13	11.3	-9.1	6.0	-2.9	1.3	0.7	1.0	-0.4	2.7	-6.5	20.5	-33.9	1423.6	-34.7	15.2	-8.5
14	-13.3	11.6	-9.0	6.0	-3.1	0.2	0.5	-1.7	3.2	2.2	-8.7	20.3	-34.7	1422.0	-27.8	18.7
15	12.4	-11.4	11.6	-9.1	6.8	-3.6	-0.5	2.0	-3.1	3.6	2.7	-4.7	15.2	-27.8	1412.5	-28.2
16	-11.7	12.4	-13.3	11.3	-7.4	3.2	1.9	-3.8	4.2	-4.2	0.7	4.5	-8.5	18.7	-28.2	1420.5

Fig. 6 Screenshot of the panel that analyzes the vibrational coupling matrix $\tilde{\boldsymbol{\Omega}}$

Table 1 Vibrational coupling matrix $\tilde{\Omega}$

	1	2	3	4	5	6	7	8	9	10	11	12	13	14	15	16
1	1,420.5	−28.2	18.7	−8.5	4.5	0.7	−4.2	4.2	−3.8	1.9	3.2	−7.4	11.3	−13.3	12.4	−11.7
2	−28.2	1,412.5	−27.8	15.2	−4.7	2.7	3.6	−3.1	2.0	−0.5	−3.6	6.8	−9.1	11.6	−11.4	12.4
3	18.7	−27.8	1,422.0	−34.7	20.3	−8.7	2.2	3.2	−1.7	0.5	0.2	−3.1	6.0	−9.0	11.6	−13.3
4	−8.5	15.2	−34.7	1,423.6	−33.9	20.5	−6.5	2.7	−0.4	1.0	0.7	1.3	−2.9	6.0	−9.1	11.3
5	4.5	−4.7	20.3	−33.9	1,423.3	−32.4	17.9	−6.7	6.3	−2.0	−1.4	0.4	1.3	−3.1	6.8	−7.4
6	0.7	2.7	−8.7	20.5	−32.4	1,426.5	−32.5	19.4	−10.7	8.0	−0.9	−1.4	0.7	0.2	−3.6	3.2
7	−4.2	3.6	2.2	−6.5	17.9	−32.5	1,422.3	−33.1	22.7	−12.4	8.0	−2.0	1.0	0.5	−0.5	1.9
8	4.2	−3.1	3.2	2.7	−6.7	19.4	−33.1	1,421.3	−32.9	22.7	−10.7	6.3	−0.4	−1.7	2.0	−3.8
9	−3.8	2.0	−1.7	−0.4	6.3	−10.7	22.7	−32.9	1,421.3	−33.1	19.4	−6.7	2.7	3.2	−3.1	4.2
10	1.9	−0.5	0.5	1.0	−2.0	8.0	−12.4	22.7	−33.1	1,422.3	−32.5	17.9	−6.5	2.2	3.6	−4.2
11	3.2	−3.6	0.2	0.7	−1.4	−0.9	8.0	−10.7	19.4	−32.5	1,426.5	−32.4	20.5	−8.7	2.7	0.7
12	−7.4	6.8	−3.1	1.3	0.4	−1.4	−2.0	6.3	−6.7	17.9	−32.4	1,423.3	−33.9	20.3	−4.7	4.5
13	11.3	−9.1	6.0	−2.9	1.3	0.7	1.0	−0.4	2.7	−6.5	20.5	−33.9	1,423.6	−34.7	15.2	−8.5
14	−13.3	11.6	−9.0	6.0	−3.1	0.2	0.5	−1.7	3.2	2.2	−8.7	20.3	−34.7	1,422.0	−27.8	18.7
15	12.4	−11.4	11.6	−9.1	6.8	−3.6	−0.5	2.0	−3.1	3.6	2.7	−4.7	15.2	−27.8	1,412.5	−28.2
16	−11.7	12.4	−13.3	11.3	−7.4	3.2	1.9	−3.8	4.2	−4.2	0.7	4.5	−8.5	18.7	−28.2	1,420.5

Table 2 Unitary transformation matrix U_{pl} values

	1,379.8	1,380.9	1,383.8	1,386.4	1,388.1	1,392.3	1,397.4	1,408.2	1,427.5	1,484.5	1,502.1	1,546.8
1,422.0	18.83	19.37	21.60	−33.79	9.67	32.11	−38.08	36.15	−37.99	40.21	22.75	−14.24
1,423.6	33.52	28.66	44.03	−34.37	23.45	18.55	1.75	−8.55	30.61	−37.12	−34.72	21.07
1,423.3	31.22	6.02	38.79	14.30	32.51	−38.89	35.04	−27.26	−0.63	22.48	39.17	−26.43
1,426.5	8.27	−29.34	24.39	38.27	31.91	−29.90	−12.46	39.78	−31.12	0.73	−36.41	32.68
1,422.3	−21.06	−47.46	20.22	13.19	33.20	24.42	−38.90	0.92	37.11	−21.09	19.79	−35.99
1,421.3	−45.12	−25.55	9.33	−28.89	34.35	24.90	25.51	−35.97	−16.56	32.47	−5.10	35.93
1,421.3	−45.10	25.57	−9.34	−28.88	34.33	−24.92	25.52	35.97	−16.56	−32.47	−5.10	−35.93
1,422.3	−21.03	47.47	−20.22	13.20	33.18	−24.45	−38.89	−0.92	37.11	21.09	19.79	35.99
1,426.5	8.29	29.33	−24.40	38.26	31.92	29.89	−12.47	−39.78	−31.12	−0.72	−36.40	−32.68
1,423.3	31.24	−6.04	−38.79	14.29	32.54	38.88	35.03	27.25	−0.63	−22.49	39.17	26.43
1,423.6	33.53	−28.67	−44.02	−34.37	23.43	−18.57	1.75	8.55	30.61	37.13	−34.71	−21.07
1,422.0	18.83	−19.37	−21.58	−33.79	9.65	−32.14	−38.08	−36.16	−37.99	−40.21	22.74	14.24
Int:	1.57e+00	1.01e+01	2.66e+00	1.02e+01	9.50e+00	6.45e−01	1.21e+00	2.24e−01	3.16e−01	2.38e−01	−1.55e−01	4.82e−01
Percent:	4.20	27.09	7.14	27.30	25.50	1.73	3.24	0.60	0.85	0.64	0.42	1.29

The localized modes l constitute the lines of the table, while the columns are the "optimum" normal modes p. The ROA backward-scattering intensities (in $Å^4$/amu) associated with the "optimum" normal modes are given at the bottom of the table together with their percentage

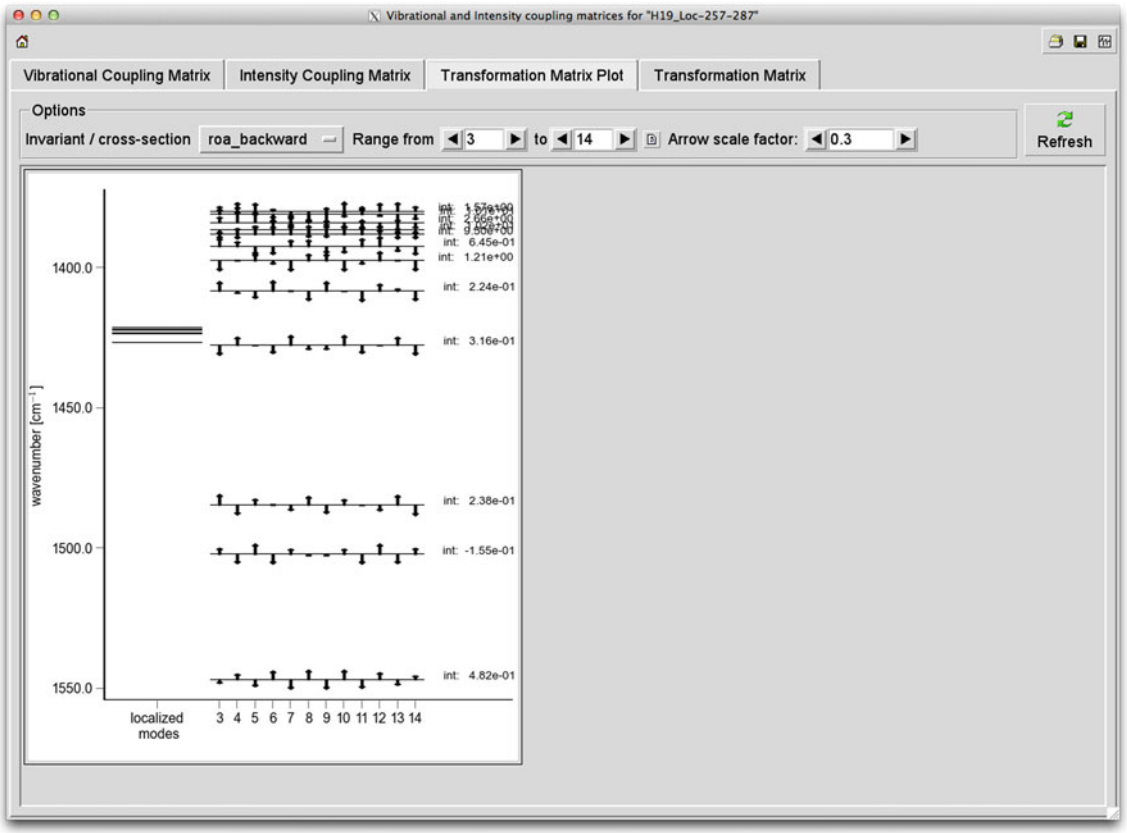

Fig. 7 Screenshot of the panel that analyzes the unitary transformation matrix $\boldsymbol{U}$ using a graphical representation of the matrix. The ROA backward-scattering intensities (in Å^4/amu) associated with the "optimum" normal modes are also given

5.4 Analysis of the vibrational and intensity coupling matrices

Now that we have obtained the localized modes, we can interpret the normal modes as combinations of the localized modes, which form a basis set. The first quantity of interest is the vibrational coupling matrix (Eq. 15), which defines the coupling (in wavenumbers) between two localized modes. We can see here the benefit of ordering the localized modes. Indeed, the coupling between modes l and $l+1$ ($\tilde{\Omega}_{l,l+1}$) now corresponds to the coupling between two localized modes that have atomic contributions on neighboring sites. Their vibrational coupling matrix is similar to the coupling matrix between two or more states. Let's consider a two-state model with two states $|\psi_1\rangle$ and $|\psi_2\rangle$ of identical energy $E = \alpha$ coupled by an interaction term $V = \beta$. The wavefunction $|\Psi_i\rangle = C_{1i}|\psi_1\rangle + C_{2i}|\psi_2\rangle$ is obtained by solving the following set of equations:

$$\begin{pmatrix} \alpha & \beta \\ \beta & \alpha \end{pmatrix} \begin{pmatrix} C_{1i} \\ C_{2i} \end{pmatrix} = \lambda_i \begin{pmatrix} C_{1i} \\ C_{2i} \end{pmatrix} \tag{21}$$

It has two solutions: $\Psi_1 = \sqrt{2}/2(\psi_1 + \psi_2)$ with $\lambda_1 = \alpha + \beta$, and $\Psi_2 = \sqrt{2}/2(\psi_1 - \psi_2)$ with $\lambda_2 = \alpha - \beta$. If the coupling β is positive, the in-phase combination is higher in energy than the out-of-phase combination, while the order is reversed when β is negative. The problem we are solving in the localized mode procedure (Eq. 15) is the reverse one. Indeed, we already know the eigenvalues of the vibrational coupling matrix $\tilde{\boldsymbol{\Omega}}$ that are the frequencies of the normal modes. By defining a criterion, we find the transformation matrix $\boldsymbol{U}$ (corresponding to the eigenvectors of $\tilde{\boldsymbol{\Omega}}$) in order to define the vibrational coupling matrix $\tilde{\boldsymbol{\Omega}}$. By doing so, we can now better understand the normal modes. For instance, in our example of the [19]helicene molecule, the vibrational coupling matrix is dominated by negative contributions from first-nearest neighbors together with smaller absolute contributions for the second-nearest neighbors (Fig. 6 and Table 1). The coupling pattern is therefore slightly more sophisticated than in the simple two-state model, but the conclusion is similar: since the most intense coupling is negative, the in-phase normal mode will be at lower wavenumber while the out-of-phase normal mode will be at higher wavenumber. This is further illustrated in Fig. 7 which sketches the positions in wavenumbers of the normal modes together with up and down arrows illustrating the contribution of each localized

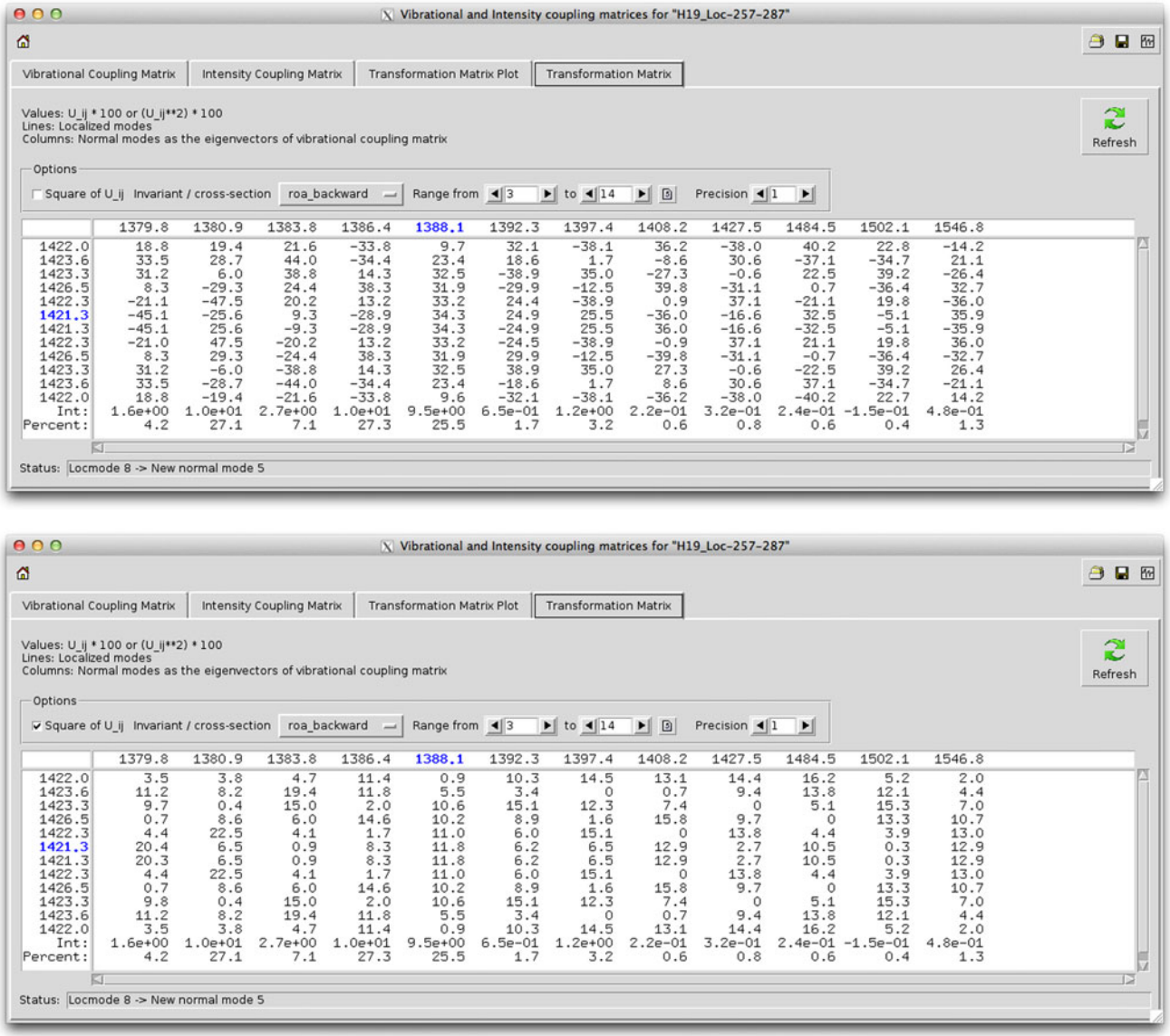

Fig. 8 Screenshot of the panel that analyzes the unitary transformation matrix $\boldsymbol{U}$. The ROA backward-scattering intensities (in Å^4/amu) associated with the "optimum" normal modes are given at the bottom of the table together with their percentage

mode to a given normal mode [obtained from the unitary matrix $\boldsymbol{U}$, Eq. 13]. One observes that the mode at 1547 cm^{-1} has alternating up and down arrows meaning an out-of-phase combination (maximum of nodes), while the modes at lower frequencies have less nodes. Figure 8 represents the unitary transformation matrix $\boldsymbol{U}$. The top figure contains the values of U_{pl}*100 while the bottom figure contains U^2_{pp}*100 values for each localized modes l (lines of the table) and each normal modes p (columns of the table). The U^2_{pl}*100 quantities correspond to the percentages of a localized modes l in a normal mode p (as well as the other way around), with the sum of all terms in each column (or each line) equal to one. From the U_{pl}*100 values, we directly see the contributions of the localized modes l to a given normal mode p. For instance, the normal mode at 1,388.1 cm^{-1} has only positive terms and therefore corresponds to the in-phase mode, while the mode at 1,546.8 cm^{-1} is the out-of-phase combination (See also Table 2).

In Figs. 7, 8, and 9, only a subset of the localized modes has been taken into account: mode 3 to mode 14 (without modes 1, 2, 15, 16). By doing so, the normal modes are not the "real" normal modes but are "optimum" normal modes constructed as the eigenvectors of a subset of the vibrational coupling matrix $\tilde{\boldsymbol{\Omega}}$. Indeed, we can choose to get rid of the localized modes that have atomic contributions localized at the two extrema of the chain in order to have a more ideal "polymer-like" coupling matrix.

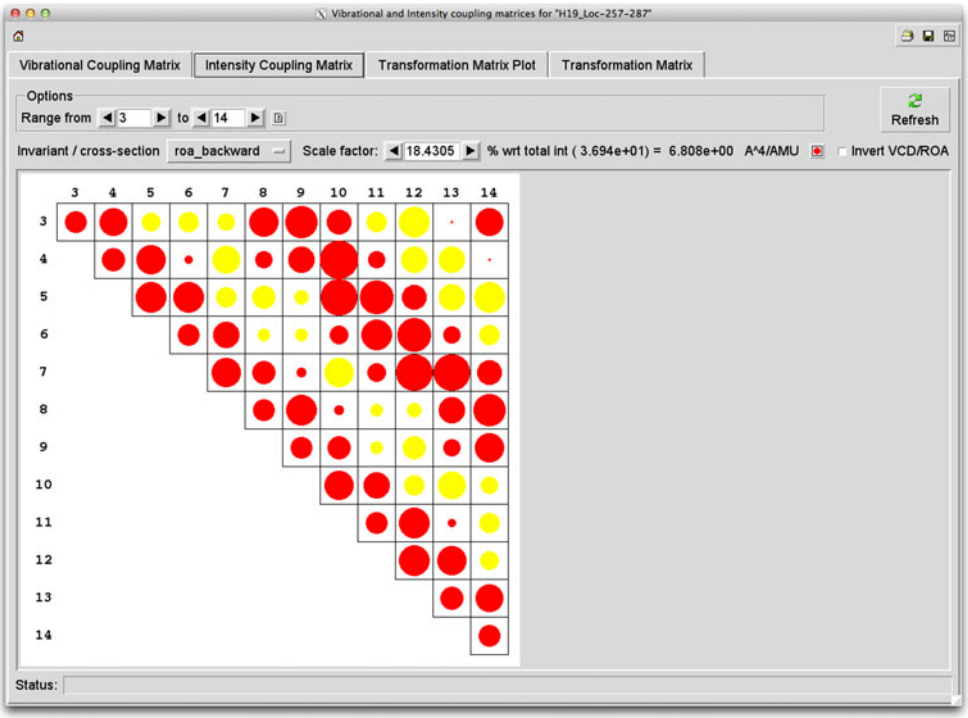

Fig. 9 Screenshot of the panel that analyzes the intensity coupling matrix $\tilde{\boldsymbol{I}}$

The eigenvectors of such subblocks of the vibrational coupling matrix $\tilde{\boldsymbol{\Omega}}$ give normal modes that are slightly different from the "real" normal modes. The intensity values given in Figs. 7 and 8 and Table 2 are therefore the intensities associated with the "optimum" normal modes and are equal to the intensity of the "real" normal modes only when all the localized modes are considered. As said before, in order to be able to have this kind of conclusion, it is crucial to have set the phase factor correctly for every localized modes.

At last, Fig. 9 is the window which represents the intensity coupling matrix ($\tilde{I}_{lm}$, Eq. 20). The diagonal elements of the matrix are the intensities associated with the localized modes, while the off-diagonal elements are the intensity coupling values. In our example, the intensity coupling terms are mostly positive with a few negative but smaller (in amplitude) contributions, which means that normal modes having a few nodes will have the highest intensities. Indeed, in Eq. (20), U_{pl} and U_{pm} will have the same sign for an in-phase normal mode p, and therefore, its intensity will be the (weighted) sum of all the terms in the intensity matrix. On the contrary, for an out-of-phase mode p, the U_{pl} and U_{pm} will have the same sign if $l = m + 2n$ and will have opposite sign if $l = m + (2n + 1)$. The intensity of such mode will therefore be the (weighted) sum of the diagonal terms of the vibrational coupling matrix minus the sum of the first off-diagonal terms plus the sum of the second off-diagonal terms minus the sum of the third off-diagonal terms, . . . Since most of these terms are positive, the different contributions will cancel out to give a very small intensity for an out-of-phase normal mode. Indeed, in Fig. 8 and Table 2, one observes that the intensity for the out-of-phase mode at 1,546.8 cm^{-1} is 20 times smaller than the intensity of the in-phase mode at 1,388.1 cm^{-1} (0.482 vs. 9.50 $Å^4$/amu).

6 Conclusions and outlook

In this paper, we have reviewed key elements for simulating and interpreting IR, Raman, VCD, and ROA spectra as well as for analyzing them by using the localized mode procedure. Then, we have presented a graphical user interface (GUI) to carry out the localization of the vibrational normal modes and have illustrated its application on the ROA spectra of the [19]helicene molecule. The overall procedure consists of four steps, and therefore, a specific interface has been designed for each of them. The first and most important part of the procedure consists in selecting the mode ensemble under which the localization procedure is performed. Then, during our step-by-step guided tour of the localized mode procedure in Pyvib2, we have highlighted the importance of the ordering of the localized modes and the importance to set correctly the phase factor between the localized modes. Finally, the vibrational coupling matrix ($\tilde{\boldsymbol{\Omega}}$), the intensity coupling matrix ($\tilde{\boldsymbol{I}}$), and the unitary transformation matrix ($\boldsymbol{U}$) can be analyzed from their representation in the different panels.

The ROA spectrum of the [19]helicene molecule is dominated by two positive peaks associated with the normal modes 251 and 252. From the localized mode procedure, we

have identified the atomic displacements of these modes as combinations of localized modes characterized by atomic displacements that look like the motion of a "claw". Moreover, the intensity coupling matrix ($\tilde{\boldsymbol{I}}$) is shown to contain mainly positive terms, which explains why it is the in-phase combination and the combination with only a few nodes that give the most intense peaks in this band. At last, the vibrational coupling term ($\tilde{\boldsymbol{\Omega}}$) between two neighboring localized modes is negative and, as a result, the normal mode which is an in-phase combination of the localized modes is situated at lower wavenumber than the out-of-phase combination. One should note that such signature (one positive peak in the 200–2,000 cm^{-1} region) is quite unusual. Indeed, the ROA spectrum presents most of the time a succession of positive and negative peaks. The specific π-electron delocalization in the helicene molecule must be responsible for this remarkable spectrum.

Other tools such as the ACP and the GCM analyses can be applied on the localized modes by using the `Generation of Intensities` option from the thumbnail of the molecule obtained from the localized mode procedure. The main advantage of using such tools on the localized modes instead on the normal modes is that the atomic displacements of the localized modes are centered on a small part of the chain on the contrary to the normal modes that are delocalized over the whole structure. This kind of analysis has been successfully used in the past to understand the difference in signature between the α-helix and the 3_{10} helix conformations of an 20-unit oligomer of alanine [14, 50, 51] or between the $(TG)_N$ and the $(GG)_N$ conformation of a 20-unit polypropylene chain [52]. Thanks to this implementation in Pyvib2, we hope that such strategy will be used to analyze the vibrational signatures of various synthetic or bio-related oligomers.

Acknowledgments The authors thank Maxim Federovsky and Werner Hug for fruitful discussions about the Pyvib2 program and Christoph Jacob and Markus Reiher for discussions about the localized mode methodology. V.L. thanks the Fund for Scientific Research (F.R.S-FNRS) for his Postdoctoral Researcher position. The calculations were performed on the Interuniversity Scientific Computing Facility (ISCF) installed at the FUNDP, for which we gratefully acknowledge financial support from the F.R.S.-FNRS (Convention No. 2.4.617.07.F), and from the FUNDP.

References

1. Quinet O, Champagne B (2002) J Chem Phys 117:2481
2. Quinet O, Champagne B, Rodriguez V (2004) J Chem Phys 121:4705
3. Mani A, Schultz Z, Caudano Y, Champagne B, Humbert C, Dreesen L, Gewirth A, White JO, Thiry PA, Peremans A (2004) J Phys Chem B 108:16135
4. Guthmuller J, Cecchet F, Lis D, Caudano Y, Mani AA, Thiry PA, Peremans A, Champagne B (2009) ChemPhysChem 10:2132
5. Liégeois V, Ruud K, Champagne B (2007) J Chem Phys 127:204105
6. Drooghaag X, Marchand-Brynaert J, Champagne B, Liégeois V (2010) J Phys Chem B 114:11753
7. Liégeois V, Champagne B (2011) J Phys Chem A 115:13706
8. Fedorovsky M (2007) Pyvib2, a program for analyzing vibrational motion and vibrational spectra. http://pyvib2.sourceforge.net
9. Frisch MJ, Trucks GW, Schlegel HB, Scuseria GE, Robb MA, Cheeseman JR, Scalmani G, Barone V, Mennucci B, Petersson GA, Nakatsuji H, Caricato M, Li X, Hratchian HP, Izmaylov AF, Bloino J, Zheng G, Sonnenberg JL, Hada M, Ehara M, Toyota K, Fukuda R, Hasegawa J, Ishida M, Nakajima T, Honda Y, Kitao O, Nakai H, Vreven T, Montgomery JA Jr., Peralta JE, Ogliaro F, Bearpark M, Heyd JJ, Brothers E, Kudin KN, Staroverov VN, Kobayashi R, Normand J, Raghavachari K, Rendell A, Burant JC, Iyengar SS, Tomasi J, Cossi M, Rega N, Millam JM, Klene M, Knox JE, Cross JB, Bakken V, Adamo C, Jaramillo J, Gomperts R, Stratmann RE, Yazyev O, Austin AJ, Cammi R, Pomelli C, Ochterski JW, Martin RL, Morokuma K, Zakrzewski VG, Voth GA, Salvador P, Dannenberg JJ, Dapprich S, Daniels AD, Farkas ö, Foresman JB, Ortiz JV, Cioslowski J, Fox DJ (2009) Gaussian 09 Revision A.1. Gaussian Inc., Wallingford, CT
10. Dalton, a molecular electronic structure program, Release Dalton2011 (2011) see http://daltonprogram.org/.
11. Hug W (2001) Chem Phys 264:53
12. Hug W, Fedorovsky M (2008) Theor Chem Acc 119:113
13. Fedorovsky M (2006) Comput Lett 2:233
14. Jacob CR, Reiher M (2009) J Chem Phys 130:084106
15. Martin RH (1974) Angew Chem Int Ed 13:649
16. Autschbach J, Patchkovskii S, Ziegler T, van Gisbergen SJA, Baerends EJ (2002) J Chem Phys 117:581
17. Furche F, Ahlrichs R, Wacksmann C, Weber E, Sobanski A, Vögtle F, Grimme S (2000) J Am Chem Soc 122:1717
18. Autschbach J, Ziegler T, van Gisbergen SJA, Baerends EJ (2002) J Chem Phys 116:6930
19. Spassova M, Asselberghs I, Verbiest T, Clays K, Botek E, Champagne B (2007) Chem Phys Lett 439:213
20. Botek E, Champagne B (2007) J Chem Phys 127:204101
21. Verbiest T, Elshocht SV, Kauranen M, Hellemans L, Snauwaert J, Nuckolls C, Katz TJ, Persoons A (1998) Science 282:913
22. Verbiest T, Sioncke S, Persoons A, Vyklicky L, Katz TJ (2002) Angew Chem Int Ed 41:3882
23. Jansík B, Rizzo A, Ågren H, Champagne B (2008) J Chem Theory Comput 4:457
24. Liégeois V, Liégeois V (2009) J Comput Chem 30:1261
25. Wilson EB, Decius JC, Cross PC (1980) Molecular vibrations: the theory of infrared and Raman vibrational spectra (Dover Books on Chemistry). Dover Publications, New York
26. Barron LD, Buckingham AD (1971) Mol Phys 20:1111
27. Hug W (2002) In: Chalmers JM, Griffiths PR (eds) Handbook of vibrational spectroscopy. Wiley, New York, p 175
28. Barron LD (2004) Molecular light scattering and optical activity, 2 edn. Cambridge University Press, Cambridge
29. Stephens PJ (1985) J Phys Chem 89:748
30. Stephens PJ (1987) J Phys Chem 91:1712
31. Cheeseman JR, Frisch MJ, Devlin FJ, Stephens PJ (1996) Chem Phys Lett 252:211
32. He Y, Bo W, Dukor RK, Nafie LA (2011) Appl Spectrosc 65:699
33. Neugebauer J, Reiher M, Kind C, Hess B (2002) J Comput Chem 23:895
34. Buckingham AD (1967) Adv Chem Phys 12:107
35. Komornicki A, Fitzgerald G (1993) J Chem Phys 98:1398
36. Hehre WJ, Ditchfield R, Pople JA (1972) J Chem Phys 56:2257
37. Scott AP, Radom L (1996) J Phys Chem 100:16502
38. Irikura KK, Johnson RD III, Kacker RN (2005) J Phys Chem A 109:8430

39. Merrick J, Moran D, Radom L (2007) J Phys Chem A 111:11683
40. Zuber G, Hug W (2004) J Phys Chem A 108:2108
41. Binkley JS, Pople JA, Hehre WJ (1980) J Am Chem Soc 102:939
42. Pecul M, Rizzo A (2003) Mol Phys 101:2073
43. Reiher M, Liégeois V, Ruud K (2005) J Phys Chem A 109:7567
44. Pecul M, Ruud K (2005) Int J Quantum Chem 104:816
45. Cheeseman JR, Shaik MS, Popelier PLA, Blanch EW (2011) J Am Chem Soc 133:4991
46. Cheeseman JR, Frisch MJ (2011) J Chem Theory Comput 7:3323
47. Perera SA, Bartlett RJ (1999) Chem Phys Lett 314:381
48. Crawford TD, Ruud K (2011) ChemPhysChem 12:3442
49. Joshi SP, Dutta AK, Pal S, Vaval N (2012) Chem Phys 403:25
50. Jacob CR, Luber S, Reiher M (2009) J Phys Chem B 113:6558
51. Jacob CR, Luber S, Reiher M (2009) Chem Eur J 15:13491
52. Liégeois V, Jacob CR, Champagne B, Reiher M (2010) J Phys Chem A 114:7198